

# Microreactor Mixing-Unit Design for Fast Liquid–Liquid Reactions

Eric Mielke<sup>1</sup>, Dominique M. Roberge<sup>2\*</sup> and Arturo Macchi<sup>1\*</sup>

<sup>1</sup>Centre for Catalysis Research and Innovation, Department of Chemical and Biological Engineering, University of Ottawa, K1N 6N5 Ottawa, Canada

<sup>2</sup>Chemical Manufacturing Technologies, Lonza AG, CH-3930 Visp, Switzerland

Received: 23 May 2016; accepted: 07 July 2016

Based on previous work studying complex microreactors, it was desired to further improve the mixing efficiency by varying the mixing unit design for fast liquid–liquid reactions. Different flow regimes were studied, including slug flow, parallel flow, and drop flow. The two-phase hydrolysis of 4-nitrophenyl acetate in sodium hydroxide solution was used to evaluate the overall volumetric mass transfer coefficients ( $K_{\text{org}}a$ ) as a function of the average rate of energy dissipation ( $\varepsilon$ ) for each microreactor design and all flow regimes. The liquid–liquid systems investigated used *n*-butanol or toluene as the organic phase solvent and a 0.5-M NaOH aqueous solution. The use of surfactant was also investigated with the toluene–water system. All microreactor geometry designs were based on contraction–expansion repeating units with asymmetric obstacles to aid the breakup of slugs and desynchronize the recombination of split streams. The investigated designs were chosen to avoid the formation of the parallel flow regime, contrary to curvature-based mixing-unit designs. The microreactor design can then be optimized to reduce the  $\varepsilon$  required to reach drop flow, since  $K_{\text{org}}a$  has been found to be constant at equal  $\varepsilon$  for a given solvent system in this flow regime, regardless of the reactor selection. Additionally, the “3/7th” scale-up rule was applied and confirmed with the LL-Triangle mixer. It was found that, for low interfacial-tension systems (i.e., *n*-butanol–water), the onset of drop flow occurred at a lower  $\varepsilon$  for the LL-Triangle mixer when compared with the Sickle or LL-Rhombus mixers.

**Keywords:** microreactor, liquid–liquid reaction, mass transfer, mixing, slug, parallel, drop, and dispersed flow

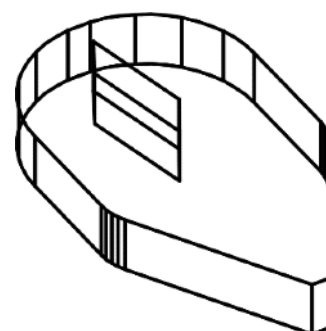
## 1. Introduction

In the past 10 years, flow technologies have become an ever more popular field of study in the fine chemical and pharmaceutical industries [1]. Continuous flow is an attractive alternative to conventional batch processing with a number of benefits, namely, process intensification via higher operating pressures and temperatures and the increased surface-to-volume ratios involved with miniaturization (microreactors). While these advantages have been studied extensively in single-phase systems [1–7], much of the research on multiphase systems [7–10] involves slug or parallel flow regimes where interphase mass transfer is relatively slow.

Previous work [11–17] studied the effects of using passive micromixing structures to increase the mass transfer rate between two immiscible phases in flow ranges that would have otherwise been in the slug flow regime for a similar-sized capillary reactor. A micromixer-based reactor was shown to be well suited for fast liquid–liquid reactions [14] (i.e., mass or heat transfer limited with reaction times in the millisecond to second range). Plouffe et al. further investigated the dependency of flow regimes on solvent-pair selection [12] and micromixer structure [11]. It was found that systems with low interfacial tension could transition from slug, to parallel, and then to drop flow regime with increasing flow rates, whereas systems with higher interfacial tension would not favor the parallel flow regime to form. Slug flow was shown to have an increasing overall volumetric mass transfer coefficient ( $K_{\text{org}}a$ ) with flow while the transition from slug to parallel flow would cause a significant drop in  $K_{\text{org}}a$  due to the decreased surface area available for interphase mass transfer. The drop flow regime was found to have the highest  $K_{\text{org}}a$  and would only increase with flow. In the study involving various reactor geometries [11], it was also shown that  $K_{\text{org}}a$  is only a function of the average rate of energy dissipation ( $\varepsilon$ ) and solvent pair once the flow has reached the drop flow regime, independent of reactor geometry, indicating that an ideal micromixer for fast liquid–liquid reactions must achieve drop flow at the lowest possible  $\varepsilon$ .

While investigating various mechanisms of mixing in micromixer, it was found that curvature-based micromixers could allow for the formation of a parallel flow regime while this was avoided in obstacle-based micromixers. Parallel flow is caused by the difference in densities between the two phases, where the denser phase would be forced to the outer edge of the curve due to centrifugal forces. When an increased rate of interphase mass transfer is desired, parallel flow should be avoided due to the reduced internal circulation in each phase, along with the reduced specific area available for mass transfer when compared with slug or drop flow regimes.

This work investigates the LL-Rhombus and LL-Triangle micromixers, which are designed as modifications to the Sickle mixer with reduced curvature while keeping a contraction–expansion and obstacle as primary modes of energy dissipation. The only difference between the LL-Rhombus and LL-Triangle (which is shown in Figure 1) is the obstacle shape, where the rhombus has a more hydrodynamic shape with a cutting angle of 42° and the triangle has an abrupt wall at a 90° angle towards the flow direction. The use of an obstacle with an angle greater than 90° and reverting flow in the opposite direction [18] was avoided as it could generate parallel flow under some conditions [11]. Another LL mixer without obstacle was tested to confirm that an obstacle is beneficial for more efficient mixing than solely relying on the contraction–expansion.



**Figure 1.** 3D visualization of the LL-Rhombus mixing element




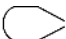
\* Authors for correspondence: dominique.roberge@lonza.com (D. M. Roberge); arturo.macchi@uottawa.ca (A. Macchi)

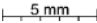
## 2. Results and Discussion

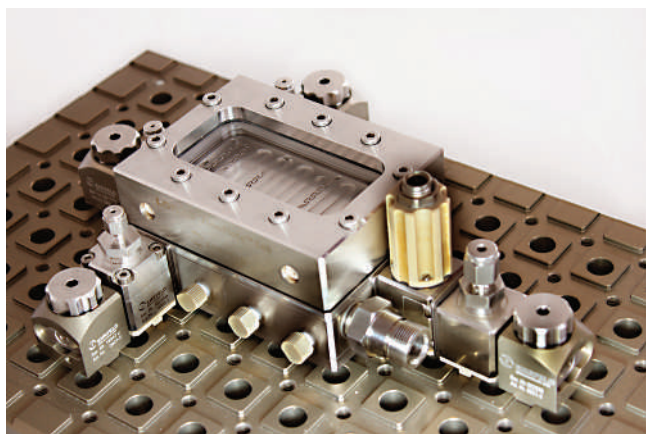
All four geometries studied and the specifications of their reactor plates can be found in Table 1. The micromixers were manufactured as exchangeable plates onto a FlowPlate® Lab (size A7, seen in Figure 2) reactor unit, which allows for visualization of the flow regimes through a glass viewport. Size 600 micromixers have a hydraulic diameter measured at the narrowest contraction,  $d_h$ , of 286  $\mu\text{m}$  (width of 0.2 mm, depth of 0.5 mm). Scaled-up versions of the LL-Rhombus and LL-Triangle were also studied, and the specifications of these reactor plates can be found in Table 2. The size 300 mixers were designed with a  $d_h$  of 714  $\mu\text{m}$  (width of 0.5 mm, depth of 1.25 mm), a diameter that allows for roughly a 10 $\times$  scale-up of flow rate for constant energy dissipation [13]. An example of both reactor plate scales can be seen in Figure 3. Note that the term reactor plate refers to an entire reactor with multiple micromixers, while mixer or mixing unit relates to a particular mixing element.

The first study compares the different geometries at the smaller scale, size 600, both visually and analytically using the alkaline hydrolysis of 4-nitrophenyl acetate. The product of the reaction, sodium 4-nitrophenolate, colors the aqueous phase yellow and allows visual distinction between the two phases and qualitatively the extent of the reaction. Toluene–water and *n*-butanol–water systems were chosen as the initially tested solvent pairs due to their widely different physical properties as shown in Table 6. Toluene–water represents a high interfacial tension system with low solubility in water (0.01 mol%) whereas *n*-butanol–water has a much lower interfacial tension and greater solubility (1.88 mol%). Using these solvents allows for the evaluation of the geometries across a wide range of experimental conditions.

**Table 1.** Size 600 micromixer geometries studied and number of mixers per plate reactor with a  $d_h$  of 286  $\mu\text{m}$  (width of 0.2 mm, depth of 0.5 mm)

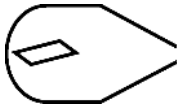

Structure	Repeating element	$N_{\text{mixer}}$	Volume (mL)
Sickle		71	0.48
LL-Rhombus		88	0.24
LL-Triangle		88	0.24
LL-Empty		88	0.25

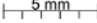




**Figure 2.** A FlowPlate® Lab reactor system setup (© Ehrfeld Mikrotechnik BTS)

**Table 2.** Size 300 micromixer geometries studied and number of mixers per plate reactor with a  $d_h$  of 714  $\mu\text{m}$  (width of 0.5 mm, depth of 1.25 mm)

Structure	Repeating element	$N_{\text{mixer}}$	Volume (mL)
LL-Rhombus		21	0.95
LL-Triangle		21	0.95



Since the LL-Triangle and LL-Rhombus geometries are similar, further comparison was performed with a toluene–water system with the presence of a surfactant, sodium dodecylbenzene sulfonate (SDBS). This was done in order to determine if the slug/drop flow regime could be eliminated in systems with interfacial tensions between that of *n*-butanol–water and toluene–water. Finally, to confirm the applicability of scale-up rules in micromixers [13], the LL-Triangle mixer was tested with *n*-butanol–water and toluene–water systems at the larger mixer size 300. In all of the studies, the main objective was to determine which micromixer could generate drop flow (and therefore highest  $K_{\text{org}a}$ ) at the lowest average rate of energy dissipation for a given solvent system.

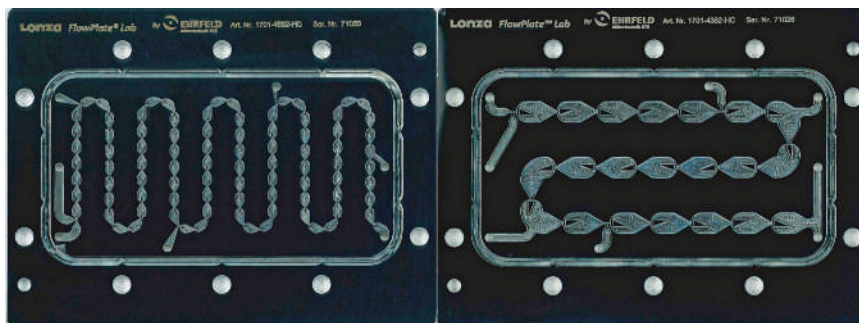
### 2.1. All Geometries Comparison

**2.1.1. Visualization of Flow Regimes.** In studying multiphase mixing in microreactors, it is important to first investigate the flow regimes that occur [11, 12, 14]. Previous work distinguished between three distinct flow regimes: slug, parallel, and drop flow [12]. In the present study, combinations of these flow regimes were observed at different flow rates in each of the reactors studied. In addition, dispersed flow is defined to be a subset of drop flow where droplets are too small to be resolved visually and are seen as an emulsion. It is important to note that this is not a meaningful change in flow regime but rather a qualitative point that can be observed visually. The flow regimes in the *n*-butanol–water systems for size 600 reactors are shown in Table 3 with the flow regime map in Figure 4.

In the Sickle reactor plate, parallel flow was observed in some form from 1.0 to 7.0 mL/min, while both LL mixers avoided this flow regime due to the minimization of curvature in the design. In fact, the LL-Triangle achieved drop flow at flow rates as low as 1.0 mL/min, whereas the LL-Rhombus required at least 3.0 mL/min.

Table 4 shows the flow regimes observed in the toluene–water system for all four geometries studied, and Figure 5 shows the flow regime map for the Sickle, LL-Rhombus, and LL-Triangle. The LL-Empty was not included in the map as it is not an obstacle-based micromixer and, therefore, has different flow regimes than the other mixers, as depicted in Table 4.

As the toluene–water system has a greater interfacial tension than *n*-butanol–water, it is expected that higher flow rates are required for the onset of drop flow. In addition, parallel flow was not likely to be observed in any micromixers with this solvent system [12]. When comparing the Sickle to the two LL mixers with obstacles, the Sickle required higher flow rates to begin the break-up of slugs. While the onset of drop flow in the Sickle mixer occurs at 8 mL/min, the LL-Rhombus and LL-Triangle were already in a slug/drop regime as early as 1.5 and 1.0 mL/min, respectively. This unstable transition regime has a significant improvement over the slug flow regime that is present in the Sickle in terms of the overall volumetric mass



**Figure 3.** Examples of size 600 (left) and 300 (right) A7 reactor plates for the FlowPlate® Lab reactor system (© Ehrfeld Mikrotechnik BTS)

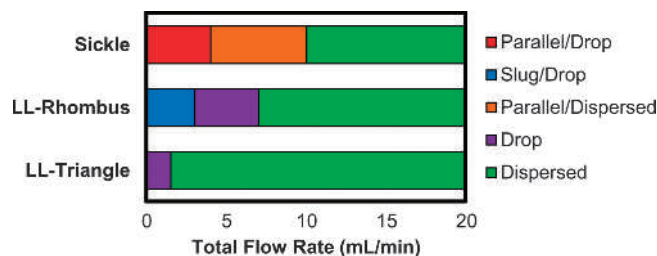
**Table 3.** *n*yButanol–water flow regimes at various flow ranges (using interval notation) for the size 600 (a) Sickle, (b) LL-Rhombus, and (c) LL-Triangle

Flow regime [Flow rate ( $\frac{\text{mL}}{\text{min}}$ )]	Visualization
(a) Sickle	
Parallel/drop [1.0–4.0]	
Parallel/dispersed [4.0–7.0]	
Dispersed [7.0–20.0]	
(b) LL-Rhombus	
Slug/drop [1.0–3.0]	
Drop [3.0–7.0]	
Dispersed [7.0–20.0]	
(c) LL-Triangle	
Drop <sup>a</sup> [1.0–1.5]	
Dispersed [1.5–20.0]	

<sup>a</sup> Video of flow regime shown in Supplementary Material V.1.

transfer coefficient, as will be discussed further. The visualization of the flow regimes in the LL-Empty (Table 4d) shows that an obstacle is required to avoid jetting through the reactor.

**2.1.2. Analytical Results from the Alkaline Hydrolysis of 4-NPA.** In addition to studying the flow regimes visually,  $K_{\text{org}}a$



**Figure 4.** Flow regimes vs. flow rate for various size 600 geometries in an *n*-butanol–water system

can be measured analytically through the test reaction of 4-NPA [11–13] with NaOH due to the fast kinetics of the reaction [19–21] and the insolubility of 4-NPA in the aqueous NaOH solution (less than 2.5 mmol/L at 23 °C). First, the different geometries are evaluated based on the conversion vs. total flow rate ( $Q_{\text{tot}}$ ). These results are presented in Figure 6 for *n*-butanol–water (a) and toluene–water (b).





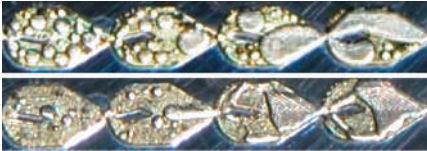



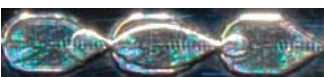

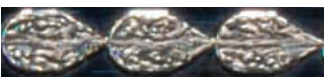
Most of the results follow a similar trend when increasing the flow rate. There is an initial decrease in conversion for the first flow rates below 3 mL/min, followed by a slight rise in conversion with flow. For *n*-butanol–water, the final increase reaches a plateau and begins to decrease with flow, whereas the conversion steadily increases with flow for the toluene–water system.

When studying these conversion data, note that there are competing factors when increasing the flow rate while in a given flow regime. Residence time decreases with flow, but the mass transfer rate increases with more energy being dissipated into the system through pressure loss. In a given flow regime, such as slug or parallel flow, the reduction in residence time is generally a greater factor, as indicated by the negative slopes in these regions. However, transitions between flow regimes can lead to a significant variation in interphase mass transfer rate, therefore, causing a pronounced change in conversion. This occurs in the transition to drop flow, where the specific area available for mass transfer increases substantially. For the toluene–water system in the drop flow regime, increasing flow can actually have an increase in conversion due to the reduction in droplet size outcompeting the reduction in residence time for flow rates above 5 mL/min.

In the toluene–water system, the LL-Triangle and LL-Rhombus perform similarly, with the exception of the slug/drop flow regime, which will be discussed further when directly comparing the two LL obstacles in section 2.2. For both solvent systems, the obstacles in the LL-Triangle and LL-Rhombus increased the conversion when compared with the LL-Empty as expected, since jetting was visible in Table 4d. This would create stagnant zones, reducing the surface area available for mass transfer.

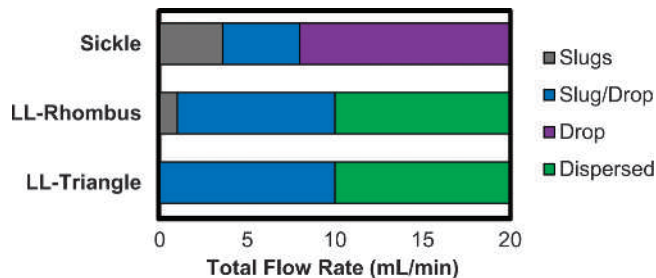
It is important to recognize that the reacting volume in the Sickle plate is roughly double that of the three LL plates, causing the conversion for the Sickle to be significantly greater.

**Table 4.** Toluene–water flow regimes at various flow ranges (using interval notation) for the size 600 (a) Sickle, (b) LL-Rhombus, (c) LL-Triangle, and (d) LL-Empty

Flow regime [Flow rate ( $\frac{\text{mL}}{\text{min}}$ )]	Visualization
(a) Sickle	
Slug [1.0–3.6]	
Slug/drop [3.6–8.0]	
Drop [8.0–20.0]	
(b) LL-Rhombus	
Slug [1.0]	
Slug/drop [1.0–10.0]	
Dispersed [10.0–20.0]	
(c) LL-Triangle	
Slug/drop <sup>a</sup> [1.0–10.0]	
Dispersed <sup>a</sup> [10.0–20.0]	
(d) LL-Empty	
Slug [1.0]	
Slug/jet/drop [1.0–5.0]	
Jet/drop [5.0–20.0]	

<sup>a</sup> Video of flow regime shown in Supplementary Material V.2.

However, the LL-Triangle results are particularly interesting, as the flow visualizations show that it achieves drop flow in


**Figure 5.** Flow regimes vs. flow rate for various size 600 geometries in a toluene–water system

*n*-butanol–water at the lowest flow rate (as seen in Table 3c and Figure 4). The benefit can clearly be seen in Figure 6a where the LL-Triangle, with half the residence time, has conversions in the range of the Sickle at low flows. The LL-Triangle also does not show any increase in conversion with flow rate because it has already reached the desired drop flow regime.

While the conversion vs. flow data is interesting in interpreting the flow regime results, it is more useful to look at the  $K_{\text{org}}a$  vs.  $\varepsilon$  since these terms normalize for reactor volume and pressure loss across the length of the reactor, allowing for the direct comparison between different micromixers. The measured conversion can be related to the overall volumetric mass transfer coefficient with eq. (1) by assuming the following: interphase mass transfer rate is fully rate-limiting; the two phases are both considered in plug flow; and no-slip velocity of the phases.

$$K_{\text{org}}a = -\frac{\phi_{\text{org}}}{\tau} \ln(1-n) \quad (1)$$

The average rate of energy dissipation is defined in eq. (2) and represents the total flow rate normalized by the reactor volume and total pressure drop. It is based on the density of the continuous phase, which is the aqueous phase due to the wetted material being stainless steel or Hastelloy C22™.

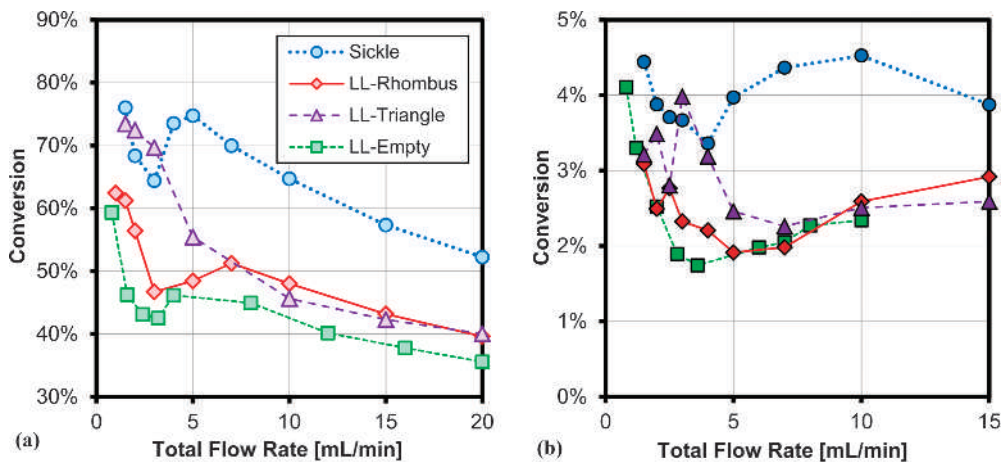
$$\varepsilon = \frac{\Delta P Q_{\text{tot}}}{\rho_c V_R} = \frac{\Delta P}{\rho_c \tau} \quad (2)$$

Comparing  $K_{\text{org}}a$  vs.  $\varepsilon$  allows for the analysis of different reactor geometries, regardless of total reactor volume or number of mixers, and highlights the most efficient geometry for generating a fine dispersion while using the least energy. The results for all four geometries with *n*-butanol–water and toluene–water can be seen in Figure 7.

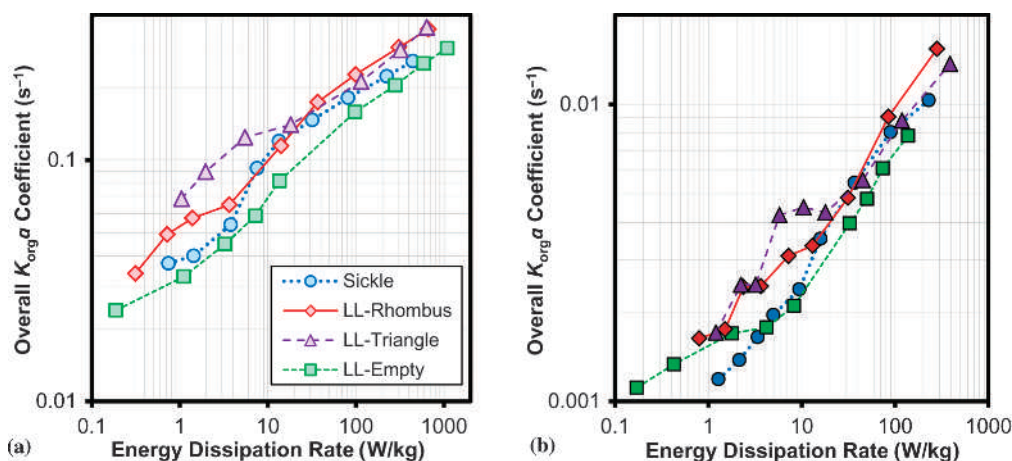
It is clear that both of the LL mixers with obstacles achieve higher  $K_{\text{org}}a$  than the Sickle and LL-Empty mixers at low flow rates. In addition, the LL-Triangle benefits significantly in the *n*-butanol–water system due to the onset of the drop flow regime at low energy dissipations. In the toluene–water system, the slug/drop flow regime shows the only difference between the LL-Triangle and LL-Rhombus. Both mixers outperform the Sickle and LL-Empty in the low flow ranges and, once all mixers have reached drop flow, the  $K_{\text{org}}a$  vs.  $\varepsilon$  converge, as expected [11].

While the LL-Empty results seem to be an exception for the convergence of  $K_{\text{org}}a$  vs.  $\varepsilon$  in drop flow, a possible explanation for the results to be consistently lower than the other plates could be due to dead zones from bypassing. This reactor volume is included in the calculation of  $K_{\text{org}}a$  and  $\varepsilon$ , but no significant reaction is occurring. This further shows that the obstacles in the LL plates allow the geometry to better utilize the reacting volume.

It is interesting to note that the results in the slug/drop flow regime are not consistent between repeated runs with the

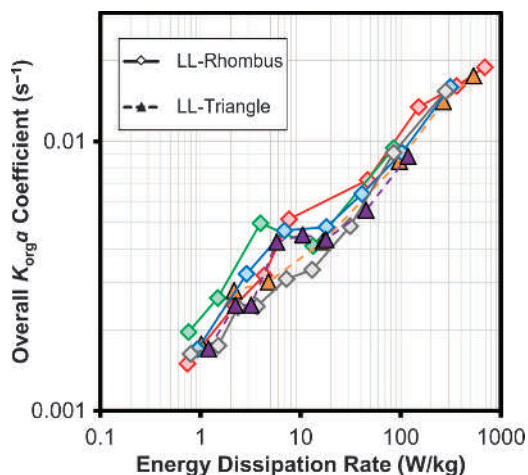


**Figure 6.** Conversion vs. total volumetric flow rate for (a) *n*-butanol–water (light) and (b) toluene–water (dark) systems with different size 600 micromixer geometries using the alkaline hydrolysis of 4-NPA



**Figure 7.** Overall volumetric mass transfer coefficient vs. the average rate of energy dissipation for (a) *n*-butanol–water (light) and (b) toluene–water (dark) systems with different size 600 micromixer geometries using the alkaline hydrolysis of 4-NPA

toluene–water. Figure 8 shows four repeated runs with the LL-Rhombus and two with the LL-Triangle. It can be seen that the point at which the flow regime transitions from slug to drop flow is not a set energy dissipation but a range between 2 and 10 W/kg. This can be considered analogous to the single-phase transition from laminar to turbulent flow where, at a given Reynolds number between 2300 and 4000, either laminar or turbulent flow is observed [22]. The actual flow regime is



**Figure 8.** Six repeated experiments for the overall volumetric mass transfer coefficient vs. the average rate of energy dissipation for toluene–water with the size 600 LL-Rhombus and LL-Triangle using the alkaline hydrolysis of 4-NPA

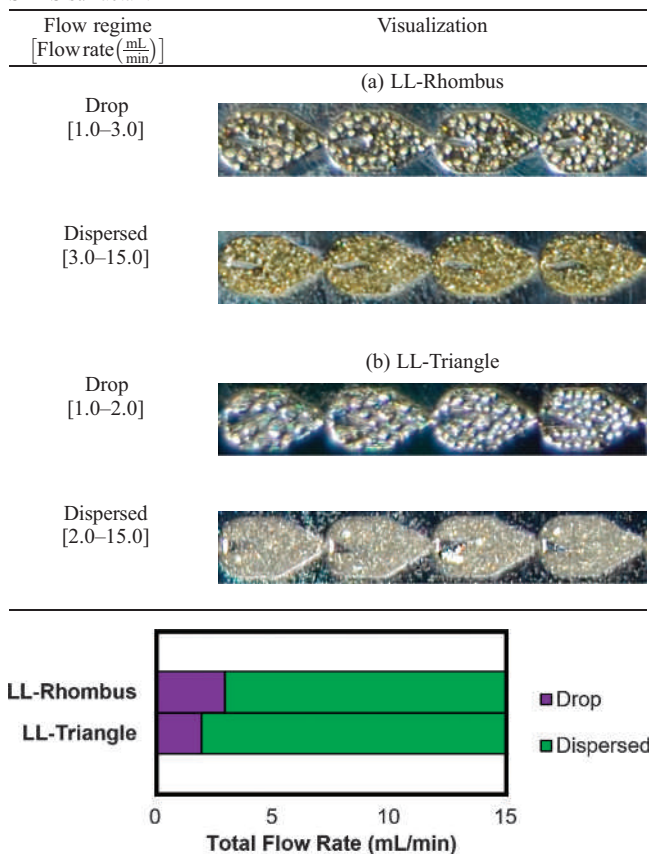
subject to environmental factors such as the uniformity of the fluid’s velocity or the wall roughness. It is possible that, in a two-phase system during the transition from slug to drop flow, the system was particularly sensitive to uncontrollable factors such as syringe changeover in the pumps (causing slight interruptions in flow every 5–30 s).

While stochastic variations from repeated experiment were sometimes observed, the specific flow regime for a given test is established readily once the flow rates from the pump achieve steady state (i.e., no lag time at start-up). Furthermore, the “development” of the flow regimes within the length of the reactor, if any, occurs in the first one to five mixing units (one for highest flow rates and five for lower flow rates as seen in V.3. in the Supporting Information).

## 2.2. Further Comparison of LL Mixers

**2.2.1. Visualization of Flow Regimes for the Toluene–Water with SDBS System.** The comparison of the LL-Triangle and LL-Rhombus was continued because of their strong performance relative to the Sickie. To accomplish this, tests were performed with a toluene–water system with the addition of the surfactant SDBS. Since droplets were formed for all flow rates in the *n*-butanol–water system, but not toluene–water, it is important to know the flow regimes for systems with interfacial tensions between those solvent pairs. The toluene–water with SDBS was investigated to determine if the slug/drop flow regime could be avoided to allow for an earlier onset of drop flow. Table 5 and Figure 9 show the observed flow regimes and flow regime map, respectively, for the LL-Rhombus and LL-Triangle reactors. Indeed, the addition of surfactant significantly reduces the flow

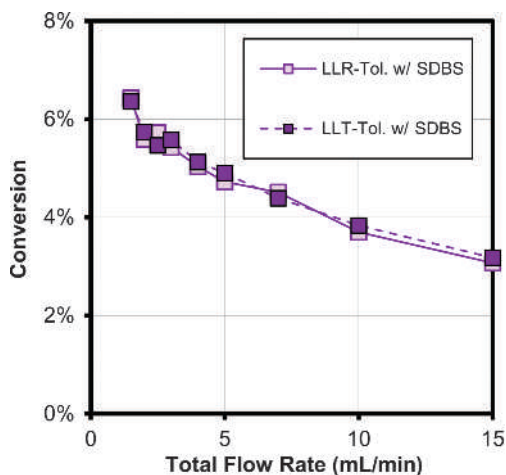
**Table 5.** Flow regimes at various flow ranges (using interval notation) for the size 600 (a) LL-Rhombus and (b) LL-Triangle with toluene–water with SDBS surfactant



**Figure 9.** Flow regimes vs. flow rate for the size 600 LL-Rhombus and LL-Triangle in a toluene–water with SDBS system

rate required for the onset of drop flow, with no tested flow rates exhibiting slug flow.

**2.2.2. Analytical Results from the Alkaline Hydrolysis of 4-NPA with the Toluene–Water with SDBS System.** The toluene–water with SDBS results for conversion vs. volumetric flow rate are presented in Figure 10. These analytical results follow expected trends since Table 5 shows that the flow regimes in both LL mixers were drop or dispersed for all flow rates tested. Since both plates have the same total volume and are in the same flow regimes for both solvent systems, it follows that the conversions should be similar as well.



**Figure 10.** Conversion vs. total volumetric flow rate for toluene–water with SDBS systems for the size 600 LL-Rhombus (LLR, light solid line) and the LL-Triangle (LLT, dark dashed line) using the alkaline hydrolysis of 4-NPA

It is worth considering all three solvent systems together for the LL-Rhombus and LL-Triangle for the  $K_{org}a$  vs.  $\epsilon$ . Figure 11 shows evidently that the two mixer geometries perform similarly in the drop flow regime, but the LL-Triangle can reach that flow regime at lower flow rates/energy dissipations. The reason for this is most likely due to the flow’s impingement against the base of the triangle obstacle, whereas the LL-Rhombus’ obstacle uses a slicing mechanism of mixing. Looking at the visualizations for the lowest flows in Table 4(b) and (c), it can be seen that the LL-Rhombus allows slugs to pass a single side of the obstacle while the LL-Triangle forces the slug to be split around it. Note that, if the obstacle forced a complete change in flow direction (e.g., a curved obstacle), this could potentially cause parallel flow due to differences in solvent densities [11].

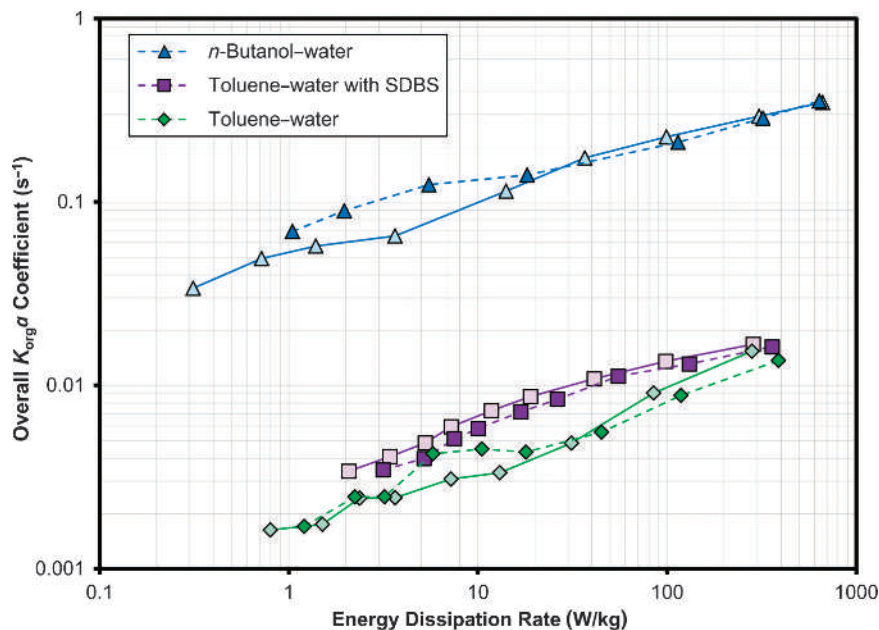
While it is interesting that the analytical results of  $K_{org}a$  for the toluene–water with SDBS system eventually converge with the system without surfactant, it is not possible to say that the droplet sizes would be equal at the highest energy dissipation. There are several factors affecting the rate of interphase mass transfer when surfactant is present. For example, the surfactant can reduce the droplet size; however, this can be counteracted by a reduction in the mass transfer coefficient across the film ( $K_{org}$ ) due to the known surface immobilization of the interface in liquid–liquid [23] and gas–liquid [24–26] systems. The key finding from testing with the surfactant was the ability to eliminate the unstable slug/drop flow regime observed in the toluene–water system and obtain consistent and repeatable mass transfer coefficients.

**2.3. Scale-up of LL Plates**

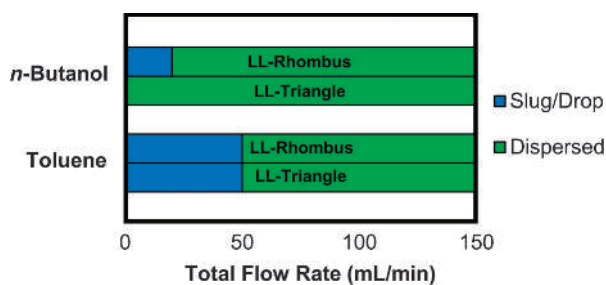
**2.3.1. Visualization of Flow Regimes.** Previous work [13] studied the scale-up of the LL-Rhombus using the “3/7th” scaling rule to maintain constant rates of energy dissipation at flow rates roughly 10 times those in the size 600. This led to mixers designed with a hydraulic diameter of 714  $\mu\text{m}$  in the size 300 mixers. Plouffe et al. showed that the scale-up of the LL-Rhombus achieved similar overall volumetric mass transfer coefficients for constant energy dissipations at both scales when in the drop flow regime. This was because the continuous phase is likely turbulent in the drop flow regime where chaotic eddies dissipate their energy partly via the creation of interfacial area, which leads to smaller drop sizes that are no longer function of the channel diameter such as for slugs. In order to confirm the application of the scale-up rule, a size 300 LL-Triangle plate was manufactured and tested with *n*-butanol–water and toluene–water systems for flow rates from 10 to 150 mL/min. Figure 12 shows the flow regime map for the various solvents; directly comparing the LL-Rhombus and LL-Triangle for the scaled-up mixers. The observed flow regimes follow a similar trend to what was seen in the size 600 mixers (with  $Q_{300} \cong 10 \times Q_{600}$ ). Again, the LL-Triangle achieved the drop flow regime at the lowest flow rate studied in *n*-butanol–water, while the flow regimes were quite similar between the two mixers for the toluene–water system. The dispersed flow regime for *n*-butanol–water in the LL-Triangle is shown in V.3. in the Supporting Information for 10 and 50 mL/min.

**2.3.2. Analytical Results from the Alkaline Hydrolysis of 4-NPA.** While the analytical results for the scale-up of the LL-Rhombus are presented in previous work [13], it is important to confirm the results for the novel LL-Triangle. Figure 13 shows the  $K_{org}a$  vs.  $\epsilon$  for both sizes 600 and 300 in *n*-butanol–water and toluene–water systems, the two systems with the widest range of interfacial tensions. While there are some differences between the two scales, particularly at low flow rates, the plates generally follow the same trend and, in the drop flow regime, converge to similar values as expected when applying the “3/7th” scaling rule.

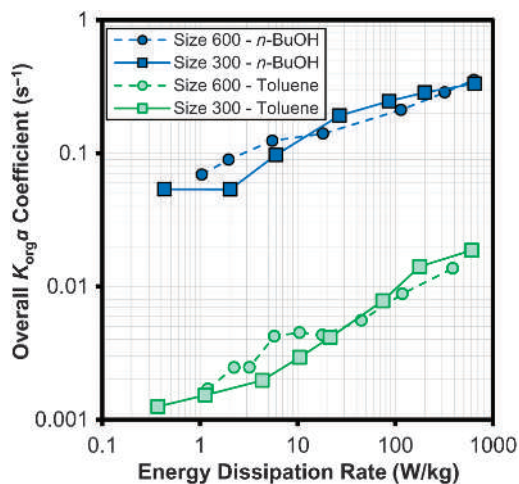
Additionally, when comparing the  $K_{org}a$  vs.  $\epsilon$  for the LL-Rhombus and LL-Triangle in the size 300 mixers, similar trends are observed as in the size 600. Figure 14 shows that the LL-Triangle is still more effective than the LL-Rhombus at low



**Figure 11.** Overall volumetric mass transfer coefficient vs. the average rate of energy dissipation with various solvents for the size 600 LL-Rhombus (light solid line) and the LL-Triangle (dark dashed line) using the alkaline hydrolysis of 4-NPA



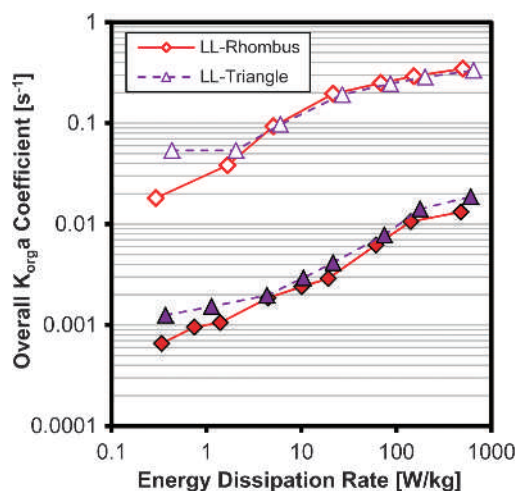
**Figure 12.** Flow regimes vs. flow rate for the size 300 LL-Rhombus and LL-Triangle in *n*-butanol-water and toluene-water systems (lowest flow rate was 10 mL/min)



**Figure 13.** Overall volumetric mass transfer coefficient vs. average rate of energy dissipation for *n*-butanol-water (dark blue) and toluene-water (light green) systems with the size 600 (○) and 300 (□) LL-Triangle mixer using the alkaline hydrolysis of 4-NPA

flows, but otherwise, they are quite similar. Not only does this further prove the applicability of the “3/7th” scale-up rule for LL-mixers but also it shows that the LL-Triangle is an effective tool for the process development of new mass-transfer-limited reactions to larger scales.

It is important to note that size 300 mixers are intended to be used on a larger microreactor system than the FlowPlate®



**Figure 14.** Overall volumetric mass transfer coefficient vs. the average rate of energy dissipation for *n*-butanol-water (light) and toluene-water (dark) systems with the size 300 LL-Rhombus and LL-Triangle using the alkaline hydrolysis of 4-NPA

Lab (size A7) and they were manufactured primarily for flow-visualization purposes. The scaled-up reactor plates can only fit 21 mixing units whereas, for example, the FlowPlate A6 system could fit 113 mixers. There is presumably a minimum number of mixers required to reach a given fully developed flow regime, and this entrance region in the size 300 A7 plate is likely significant when comparing with results from size 600 plates.

Additionally, the FlowPlate® Lab (size A7) system inlet and outlet ports are on the same order of magnitude in hydraulic diameter as the size 300 mixers, and with the higher flows being studied, it is no longer applicable to assume that the energy dissipation, and therefore the mixing, in the outlet is negligible.

### 3. Conclusions

Several obstacle-based micromixer geometries were studied with up to four different solvent-pair systems for two different mixer sizes. The liquid-liquid systems were observed and classified based on some combination of the following flow

regimes: slug flow, parallel flow, or drop flow. For applications in fast liquid–liquid reactions, drop flow is the ideal flow regime due to the increased specific area available for inter-phase mass transfer. The alkaline hydrolysis of 4-nitrophenyl acetate was used as a test reaction to measure analytically the overall volumetric mass transfer coefficients in the various mixers. The micromixers were evaluated based on the  $K_{\text{org}}a$  plotted vs. the average rate of energy dissipation to determine the most efficient mixer design (i.e., the mixer with the earliest onset of drop flow).

In the flow range of 1–20 mL/min, the novel LL-Triangle micromixer design was shown to perform equally well as or better than any of the other micromixers studied in all solvent pairs investigated, namely, the Sickle, the LL-Rhombus, and the LL-Empty. The benefits for this mixer were most clearly observed at low flow rates for low interfacial tension systems, such as *n*-butanol–water, where the drop flow regime was observed at the lowest energy dissipation. In the toluene–water system, both LL-mixers performed similarly, with a slug/drop flow regime observed for low flows. It was possible to avoid this transition regime with the use of a surfactant in the toluene–water system. Drop flow was observed in both LL-mixers at lower energy dissipations than the Sickle mixer, and unwanted parallel flow was avoided due to the reduced curvature.

The results were reproduced in a larger scale LL-Triangle for flow rates between 10 and 150 mL/min where the LL-Triangle achieved drop flow again for all flow rates studied in *n*-butanol–water. The overall volumetric mass transfer coefficients were similar to those obtained at equal energy dissipations in the smaller scale in the drop flow regime, indicating that the LL-Triangle micromixer is excellent for the process development and scale-up of fast liquid–liquid reactions. Finally, for liquid–liquid reactive systems, this work nicely shows that a flow visualization is of prime importance to enable determination of the proper flow regime and ensure consistent scale-up.

## 4. Experimental

The experimental and HPLC analytical methods used are similar to those used in previous work by Plouffe et al. [11–13] with differences in the specific reactor plates and solvents used. The specifications for the specific reactor plates can be found in Tables 1 and 2.

### 4.1. Equipment Setup

**4.1.1. Size 600 Experimental Setup.** For the size 600 tests, the Ehrfeld MMRS was used with Lonza FlowPlate® Lab reactors made from either stainless steel 316 or Hastelloy C22™. The setup can be seen in Figure 15. The system was fed the aqueous and organic solutions using two Syrdos (HiTec Zang) pumps with 5 or 2.5 mL syringes. Endress-Hauser Coriolis flow meters were used to measure the mass flow rates, and 25 or 6 bar Wika M-11 pressure transducers measured the pressure difference from the inlet to the outlet of the reactor. The system was kept at ambient temperatures using a Huber Ministat 125 thermal bath.

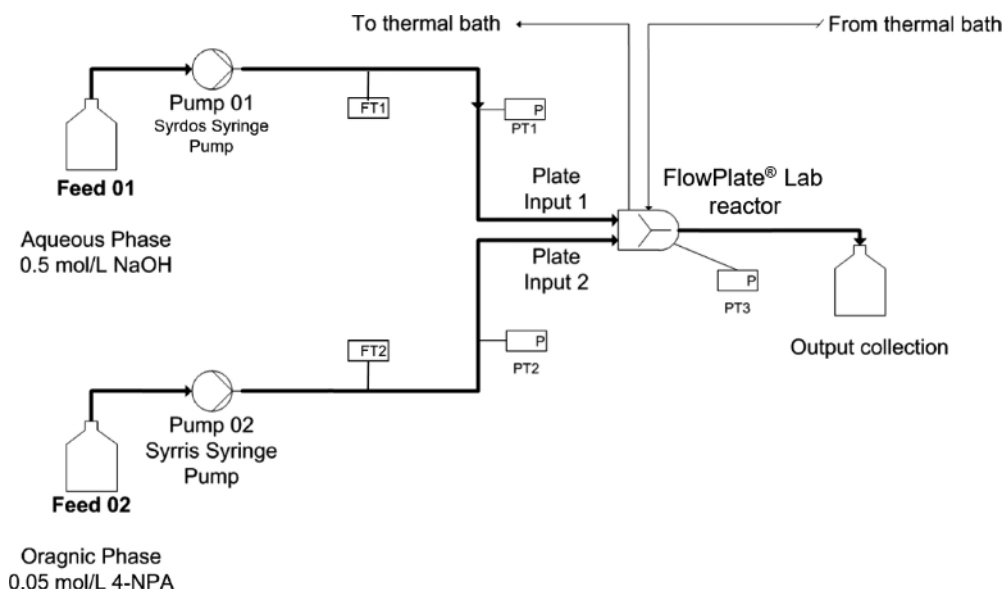
**4.1.2. Size 300 Experimental Setup.** The setup for the size 300 scaled-up mixers was identical for the size 600, except that Ismatec Reglo-Z gear pumps were used for the higher flow rates.

**4.1.3. Solvent Systems.** The physical properties of the aqueous and organic phases used can be found in Table 6. For tests with sodium dodecylbenzene sulfonate (SDBS), 0.018 g of SDBS was added to 1 L of 0.5 M NaOH solution. This was an arbitrary amount chosen after visually testing the mixing of different concentrations of SDBS in toluene–water solutions. The SDBS was added to the aqueous phase to avoid the risk of any reaction between the surfactant and the 4-NPA reactant before entering the reactor. The feed solution was kept mixed to ensure the SDBS concentration remained constant during the experiment.

**4.2. Test Reaction: Alkaline Hydrolysis of 4-Nitrophenyl Acetate.** The two-phase alkaline hydrolysis of 4-nitrophenyl acetate (4-NPA, Scheme 1) was used to analytically measure the overall volumetric mass transfer coefficient of a given mixer. It has been shown that the kinetics have an intrinsic rate constant of 14.0 L/(mol s) for a second order reaction [19–21]. Using a 0.5 mol/L concentration of NaOH in water and 0.05 mol/L of 4-NPA in whichever organic solvent was being tested allowed for a 10:1 molar ratio of NaOH to 4-NPA (due to equal volumetric flow rates), causing pseudo-first order reaction

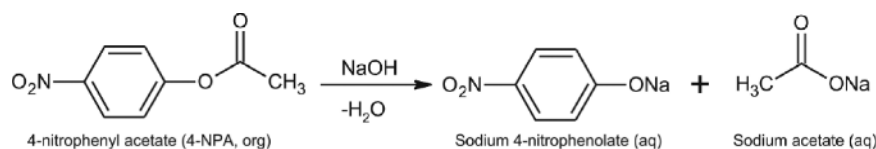
**Table 6.** Physical properties of solvents at 23 °C

Fluid	$\rho$ (kg/m <sup>3</sup> )	$\mu$ mPa s	Interfacial tension with water (mN)	Solubility in water (mol%)
Toluene [27–29]	862	0.552	35.4	0.01
<i>n</i> -Butanol [27–29]	806	2.571	1.8	1.88
0.5 M NaOH in water [30]	1020	1.124	–	–



**Figure 15.** Size 600 microreactor experimental setup



**Scheme 1.** Alkaline hydrolysis of 4-nitrophenyl acetate

conditions. In addition, the product, 4-nitrophenolate, would turn the alkaline aqueous phase yellow when present, allowing for a visual distinction of the extent of reaction. Flow visualizations were taken using the reactor sight glass with a Nikon D40x “kit” camera fitted with an AF-S DX Zoom-Nikkor 18–55 mm *f*/3.5–5.6 G ED II lens, and the flow regimes were noted.

A single experiment consisted of 7–9 flow rates being tested after flushing the system with reactants for 5 min at 10 mL/min. Once a new flow rate was set, the system was left at least three residence times to reach steady state before taking the sample. If three residence times last less than 2 min, 2 min was left between the change of flow rate and sampling to give the operator sufficient time to prepare the next sample or take photographs of the flow regime if required. The sample time for a given flow rate was the largest of three residence times or 5 s. Samples were taken at the outlet into a quench solution: an agitated mixture of acetonitrile, water, and acetic acid that homogenized and neutralized the reactor effluent. The quench solution composition was based on the particular solvent since different amounts of acetonitrile are required to homogenize the outlet sample. The samples were analyzed with an HP Agilent 1100 series HPLC system with a 250 mm × 4.6 mm i.d. Agilent Zorbax SB-C8 at room temperature.

## Nomenclature

General	Symbol	Description (units)
	$a$	specific interfacial area of contact ( $m^2/m^3$ )
	$b$	width of the channel at contraction (m)
	$d_h$	hydraulic diameter at contraction = $2hb/(h + b)$ (m)
	$h$	depth of the channel at contraction (m)
	$K$	overall convective mass transfer coefficient (m/s)
	$Q$	volumetric flow rate ( $m^3/s$ )
	$V$	volume ( $m^3$ )
	$\Delta P$	pressure drop across the reactor (Pa)

## Greek symbols

$\varepsilon$	average rate of energy dissipation (W/kg)
$\eta$	conversion (%)
$\mu$	fluid viscosity (Pa · s)
$\rho$	fluid density ( $kg/m^3$ )
$\sigma$	fluid interfacial tension with water (N/m)
$\tau$	average residence time (s)
$\varphi$	volumetric phase fraction

## Subscripts

aq	aqueous phase
c	continuous phase
d	dispersed phase
org	organic phase
tot	total (sum of organic and aqueous phase)
R	reactor
300	in a size 300 micromixer; $d_h = 714 \mu m$
600	in a size 600 micromixer; $d_h = 286 \mu m$

**Acknowledgments.** The authors would like to thank the Natural Sciences and Engineering Research Council of Canada, including the CREATE program in Continuous Flow Science, and Lonza AG for their financial contribution. Also,

Ehrfeld Mikrotechnik BTS is acknowledged for the reactor manufacturing.

**Open Access.** This article is distributed under the terms of the Creative Commons Attribution 4.0 International License (<https://creativecommons.org/licenses/by/4.0/>), which permits unrestricted use, distribution, and reproduction in any medium, provided the original author and source are credited, you give a link to the Creative Commons License, and indicate if changes were made.

## Supporting Information

Supplementary videos of various flow regimes (V.1., LL-Triangle — n-Butanol-water.mp4; V.2., LL-Triangle — Toluene-water.mp4; V.3., LL-Triangle Size 300 — n-Butanol-water.mp4) associated with this article can be found in the online version at doi: 10.1556/1846.2016.00026.

## References

- Kumar, V.; Parashivoiu, M.; Nigam, K. D. P. *Chem. Eng. Sci.* **2011**, *66*, 1329–1373.
- Holvey, C. P.; Roberge, D. M.; Gottsponer, M.; Kockmann, N.; Macchi, A. *Chem. Eng. Process. Process Intensif.* **2011**, *50*, 1069–1075.
- Plouffe, P.; Anthony, R.; Donaldson, A.; Roberge, D. M.; Kockmann, N.; Macchi, A. In *ASME 2012 10th International Conference on Nanochannels, Microchannels, & Minichannels*; Rio Grande, Puerto Rico, 2012.
- Kockmann, N.; Gottsponer, M.; Roberge, D. M. *Chem. Eng. J.* **2011**, *167*, 718–726.
- Kashid, M.; Renken, A.; Kiwi-Minsker, L. *Chem. Eng. J.* **2011**, *167*, 436–443.
- Falk, L.; Commenge, J. M. *Chem. Eng. Sci.* **2010**, *65*, 405–411.
- Hessel, V.; Kralisch, D.; Kockmann, N.; Noel, T.; Wang, Q. *ChemSusChem* **2013**, *6*, 746–789.
- Ducry, L.; Roberge, D. M. *Angew. Chem., Int. Ed.* **2005**, *44*, 7972–7975.
- Kashid, M. N.; Kiwi-Minsker, L. *Ind. Eng. Chem. Res.* **2009**, *48*, 6465–6485.
- Dummann, G.; Quittmann, U.; Gröschel, L.; Agar, D. W.; Wörz, O.; Morgenschweis, K. *Catal. Today* **2003**, *79–80*, 433–439.
- Plouffe, P.; Roberge, D. M.; Macchi, A. *Chem. Eng. J.* **2016**, *300*, 9–19.
- Plouffe, P.; Roberge, D. M.; Sieber, J.; Bittel, M.; Macchi, A. *Chem. Eng. J.* **2016**, *285*, 605–615.
- Plouffe, P.; Bittel, M.; Sieber, J.; Roberge, D. M.; Macchi, A. *Chem. Eng. Sci.* **2016**, *143*, 216–225.
- Plouffe, P.; Macchi, A.; Roberge, D. M. *Org. Process Res. Dev.* **2014**, *18*, 1286–1294.
- Nieves-Remacha, M. J.; Kulkarni, A. A.; Jensen, K. F. *Ind. Eng. Chem. Res.* **2013**, *52*, 8996–9010.
- Lavric, E. D.; Woehl, P. *Chem. Today* **2009**, *27*, 45–48.
- Kashid, M. N.; Renken, A.; Kiwi-Minsker, L. *Ind. Eng. Chem. Res.* **2011**, *50*, 6906–6914.
- Nieves-Remacha, M. J.; Kulkarni, A. A.; Jensen, K. F. *Ind. Eng. Chem. Res.* **2012**, *51*, 16251–16262.
- Parker, V. D. *J. Phys. Org. Chem.* **2006**, *19*, 714–724.
- Ahmed-Omer, B.; Barrow, D.; Wirth, T. *Chem. Eng. J.* **2008**, *135*, S280–S283.
- Ahmed, B.; Barrow, D.; Wirth, T. *Adv. Synth. Catal.* **2006**, *348*, 1043–1048.
- Potter, M. C.; Wiggert, D. C.; Ramadan, B. H. *Mechanics of Fluids*, 4th ed.; Cengage Learning: Stamford, CT, 2011.
- Clift, R.; Grace, J. R.; Weber, M. E. *Bubbles, Drops, and Particles*; Dover Publications, Inc.: Mineola, New York, 1978.
- Koide, K.; Yamazoe, S.; Harada, S. *J. Chem. Eng. Japan* **1985**, *18*, 287–292.
- Jeng, J. J.; Maa, J. R.; Yang, Y. M. *Ind. Eng. Chem. Process Des. Dev.* **1986**, *25*, 974–978.
- Eckenfelder, W. W.; Barnhart, E. L. *AIChE J.* **1961**, *7*, 631–634.
- Backes, H. M.; Ma, J. J.; Bender, E.; Maurer, G. *Chem. Eng. Sci.* **1990**, *45*, 275–286.
- Berthod, A.; Schmitt, N. *Talanta* **1993**, *40*, 1489–1498.
- Donahue, D. J.; Bartell, F. E. *J. Phys. Chem.* **1952**, *56*, 480–484.
- Alexandrov, A. A. *14th Int. Conf. Prop. Water Steam* **2005**, 86–90.